



This open access document is posted as a preprint in the Beilstein Archives at <https://doi.org/10.3762/bxiv.2024.39.v1> and is considered to be an early communication for feedback before peer review. Before citing this document, please check if a final, peer-reviewed version has been published.

This document is not formatted, has not undergone copyediting or typesetting, and may contain errors, unsubstantiated scientific claims or preliminary data.

Preprint Title Homogeneous continuous-flow nitration of O-methylsouronium sulfate and its optimization by kinetic modeling

Authors Jiapeng Guo, Weike Su and An Su

Publication Date 11 Juni 2024

Article Type Full Research Paper

Supporting Information File 1 Supplementary Material Manuscript-Jiapeng-240521-G.docx; 1.8 MB

ORCID® IDs An Su - <https://orcid.org/0000-0002-6544-3959>



License and Terms: This document is copyright 2024 the Author(s); licensee Beilstein-Institut.

This is an open access work under the terms of the Creative Commons Attribution License (<https://creativecommons.org/licenses/by/4.0>). Please note that the reuse, redistribution and reproduction in particular requires that the author(s) and source are credited and that individual graphics may be subject to special legal provisions.

The license is subject to the Beilstein Archives terms and conditions: <https://www.beilstein-archives.org/xiv/terms>.

The definitive version of this work can be found at <https://doi.org/10.3762/bxiv.2024.39.v1>

Homogeneous continuous-flow nitration of *O*-methylisouronium sulfate and its optimization by kinetic modeling

Jiapeng Guo^a, Weike Su^a, An Su^{a, b, *}

^a Key Laboratory of Pharmaceutical Engineering of Zhejiang Province, Key Laboratory for Green Pharmaceutical Technologies and Related Equipment of Ministry of Education, Collaborative Innovation Center of Yangtze River Delta Region Green Pharmaceuticals, Zhejiang University of Technology, Hangzhou, 310014, P. R. China

^b State Key Laboratory Breeding Base of Green Chemistry-Synthesis Technology, Key Laboratory of Green Chemistry-Synthesis Technology of Zhejiang Province, College of Chemical Engineering, Zhejiang University of Technology, Hangzhou, Zhejiang 310014, China

***Corresponding Author:**

Prof. An Su

<https://orcid.org/0000-0002-6544-3959>

Email: ansu@zjut.edu.cn

ABSTRACT

Nitration of *O*-methylisouronium sulfate under mixed acid conditions gives *O*-methyl-*N*-nitroisourea, a key intermediate of neonicotinoid insecticides with high application value. The reaction is a fast and highly exothermic process with a high mass transfer resistance, making its control difficult and risky. In this paper, a homogeneous continuous-flow microreactor system was developed for the nitration of *O*-methylisouronium sulfate under high concentrations of mixed acids, with a homemade static mixer eliminating the mass transfer resistance. In addition, the kinetic modeling of this reaction was performed based on the theory of NO_2^+ attack, with the activation energy and pre-exponential factor determined. Finally, based on the response surface generated by the kinetic model, the reaction was optimized with a conversion of 87.4 % under a sulfuric acid mass fraction of 94 %, initial reactant concentration of 0.5 mol/L, reaction temperature of 40 °C, molar ratio of reactants at 4.4:1, and residence time of 12.36 minutes.

Keywords

Nitration; Continuous flow; Static mixer; Kinetic modeling; Reaction optimization

1. Introduction

The demand for high-quality insecticides is increasing as the world's food crisis intensifies due to the changes in the natural environment and ongoing geopolitical crises.[1] *O*-Methyl-*N*-nitroisoureas (NIO) is a pivotal pesticide intermediate in the preparation of nitroguanidine derivatives, which are the raw material for highly effective and non-toxic neonicotinoid insecticides, such as dinotefuran and clothianidin.[2-4] Currently, the industrial production of *O*-methyl-*N*-nitroisourea usually involves the nitration of *O*-Methylisouronium sulfate (IO) with a mixture of sulfuric acid (H₂SO₄) and nitric acid (HNO₃) in a batch reactor.[3] The reaction is a typical aliphatic nitration, which is fast and highly exothermic, requiring low reaction temperatures. In addition, the safety hazard of this reaction increased by using concentrated nitric and sulfuric acids. Therefore, it is necessary to modify the nitration reaction process of *O*-Methylisouronium sulfate to improve the reaction efficiency and intrinsic safety.

In recent years, continuous flow microreactors have been recognized due to their excellent mass and heat transfer performance, precise control over reaction parameters, and intrinsic safety.[5-8] Guo et al. constructed a continuous flow microsystem for *o*-xylene nitration and proved the process safety of *o*-xylene nitration by the adiabatic temperature rise of the nitration reaction and the characteristic heat transfer time of the microreactor.[9] The residence time of the microreactor was reduced by an order of magnitude and the volumetric mass transfer coefficient was increased by several orders of magnitude compared with that of a conventional stirred tank reactors. Jin et al. developed a continuous flow microreactor system for non-homogeneous nitration of nitrobenzene using mixed acids.[10] The reaction time and temperature were reduced from >2 h and 80 °C in industrial operation to 10 min and 65 °C in the microreactor with high conversion and selectivity. Since *O*-methylisoureonium sulfate can be dissolved in high concentrations of sulfuric acid, it is expected to construct a homogeneous continuous-flow nitration system, leading to better elimination of the

effects of mass and heat transfer.[11]

Kinetic modeling is a classical approach to chemical reaction optimization, where the effects of various reaction parameters on the results are effectively quantified by mathematical formulas, thus providing an efficient guide to optimize reaction conditions.[12] Yao et al. constructed a kinetic model on thermal dissociation and oligomerization of dicyclopentadiene (DCPD) in a continuous flow microreactor.[13] Where cyclopentadiene was the target intermediate formed by the thermal dissociation of dicyclopentadiene, cascade oligomerization was a side reaction to be avoided. Based on the deep understanding of the kinetic differences between thermal dissociation and oligomerization, the residence time and temperature were designed rationally to improve the yield of cyclopentadiene. Since NO_2^+ is the actual substance that plays a role in the nitrification process,[14] kinetic modeling based on the concentration of NO_2^+ is essential for the understanding of the nitrification mechanism and optimization reaction. Luo et al. have carried out extensive research on this topic and accurately obtained kinetic data for the nitration of chlorobenzene,[15] *o*-nitrotoluene,[16] and *p*-nitrotoluene[17] by constructing a homogeneously continuous flow reaction system. Therefore, it is feasible to model homogeneous nitrification and optimize the reaction in a continuous flow system based on NO_2^+ .

An important prerequisite for kinetic modeling is the elimination of mass and heat transfer. The effect of mass transfer resistance is greater for highly viscous reaction systems, especially at higher reactant concentrations. It is still difficult to eliminate the mass transfer effect using conventional microreactors,[18] leading to errors in the determination of nitration kinetics. Therefore, more efficient mixers are needed to eliminate the effects of mass and heat transfer. According to the mixing principle, there are active mixers and passive mixers.[19] Passive mixers do not require overly complex equipment and external energy inputs and are extensively used in continuous flow reactions.[20, 21] Passive mixers enhance the passive mixing of the liquid-liquid two-phase mass transfer process on a microscopic scale, mainly by optimizing the

microchannel geometry,[22] addition of in-channel obstacles, etc.[23-25] Santana et al. designed an efficient fluid mixer "Elis" consisting of internal walls and circular obstacles. This static mixer achieves efficient mixing in a wide range of Reynolds numbers at the micro- and milli scale.[26] However, many static mixer designs are structurally complex and require the use of 3D printing technology to aid in their manufacture, which is more expensive to use. Kilcher et al. investigated in detail the efficient mixing of organic phases (cyclopentadiene, 1,2-dichloroethane, and MeBu₃NCl) and aqueous phases (30 % NaOH) and optimized it by the use of a simple homemade "PTFE Raschig ring static mixer" (RRSM).[27] The RRSM is simple in structure, easy to fabricate, inexpensive for many flow reaction systems, and has a promising application.

In this work, we constructed a continuous flow microreactor system to determine the kinetic parameters of IO nitration, which allows precise control of temperature and residence time. (Fig. 1) Due to the high viscosity of the reaction system, a simple and practical static mixer was designed to eliminate the effect of mass transfer on the kinetic measurements and validated experimentally. We developed a kinetic model for the nitration of *O*-Methylisouronium sulfate and optimized the reaction conditions for conversion rates, which is crucial for theoretical significance and practical value for process optimization.

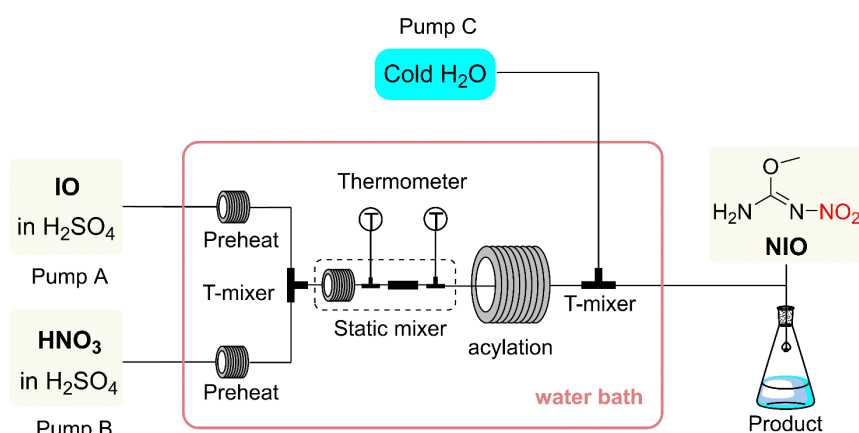


Figure 1. The schematic diagram of the Continuous flow microreactor system.

2. Materials and methods

2.1 Chemicals

O-Methylisouronium sulfate (IO, 95 %) Purchased from Shanghai Yien Chemical Technology Co., Ltd; Fuming Nitric acid (HNO₃, 98.0 %) Purchased from Sinopharm Chemical Reagent Co., Ltd.; Sulfuric acid (H₂SO₄, 98.0 %) Purchased from Sinopharm Chemical Reagent Co., Ltd.; Pure water (H₂O, AR, Hangzhou Wahaha Group Co., Ltd.); All reagents were used without further purification. Sulfuric acid solutions of different mass fractions are prepared with pure water and 98 % concentrated sulfuric acid in an ice bath with stirring.

Solution A (IO): IO (0.1 mol, 24.64 g) was dissolved in H₂SO₄ (100 mL) under stirring conditions in an ice bath, solution volume $V_A=118$ mL.

Solution B (H₂SO₄ + HNO₃): HNO₃ (0.44 mol, 18.49 mL) was dissolved in H₂SO₄ (100 mL) under stirring conditions in an ice bath, solution volume $V_B=112$ mL.

2.2 Continuous flow microreactor system

The continuous flow microreactor system is shown in Fig. 1(a). Solutions A and B were stored in two glass vials (500 mL) with lids and were preheated by two high-pressure PTFE pumps (Pump A, Pump B, JJRZ-10004F, Hangzhou JingJin Technology Co., Ltd.) pumped into coiled stainless steel capillary tubes (SS316L, 1/16-inch diameter) that were sufficiently long (1 m). After being preheated to the reaction temperature, the material was first initially mixed in a T-mixer (SS316L, 1/16-inch diameter), followed by a homemade static mixer at the outlet of the T-mixer to fully mix the material. The reaction coil (SS316L, 1/8-inch diameter) was connected directly to the outlet of the homemade static mixer, nitration took place in the reaction coil. The residence time was precisely controlled by changing the flow rate of the reaction mixture or the length of the reaction coil. All preheat tubes, mixers, and reaction coils were immersed in the same water bath to maintain a constant temperature. Finally, after controlling the

residence time, the reaction was terminated by pumping excess pure ice water through a high-pressure PTFE pump (Pump C, JJRZ-10004F, Hangzhou Jingjin Technology Co., Ltd.) into the second T-mixer.

The homemade static mixer consisted of two different mixing units as shown in Fig. 1(b) (total internal volume: 1.3154 mL). The first mixing unit consists of a section of stainless steel coil (SS316L, 1/16-inch diameter, Beijing Xiongchuan Technology Co. Ltd.) and an electronic thermometer (Beijing Xiongchuan Technology Co. Ltd.). The second mixing unit consisted of a section of PTFE piping filled with SiO₂ beads (SiO₂ beads, 3 mm diameter; piping, 1/4-inch diameter, 10 cm length, Wuxi Hongxin Special Material Technology Co.) and an electronic thermometer connected to the outlet.

2.3 Sample analysis

When the continuous flow system was operated to a steady state (after 2-3 times the residence time), the reaction solution was quenched and diluted by a large amount of ice water at the outlet of the reaction system. The quenched and diluted reaction solution was collected and analyzed by high-performance liquid chromatography (HPLC, ThermoFisher Ulcel3000), and the conversion of the samples was derived from the external standard method based on the regression equation of the HPLC standard curve. HPLC detection conditions C18 column (10 μm, 4.6×250 mm, Welch Materials Shanghai, China), the mobile phase was 80 % MeOH and 20 % ultrapure water at a flow rate of 1 mL/min, and the detection wavelength was 195 nm. The conversion of IO was calculated by the following equation:

$$x_{\text{IO}} = \left(1 - \frac{c_{\text{IO}}}{c_{\text{IO}} + c_{\text{NIO}}}\right) \quad (1)$$

The residence time was calculated as follows:

$$t = \frac{V}{Q_{\text{IO}} + Q_{\text{HNO}_3}} \quad (2)$$

where t is the reaction residence time and V is the volume of the microchannel. Q_{IO} and Q_{HNO_3} are the volume flow rates of the raw material aqueous solution, respectively. Samples were tested three times under the same conditions and averaged

to minimize errors.

2.4. Batch reaction

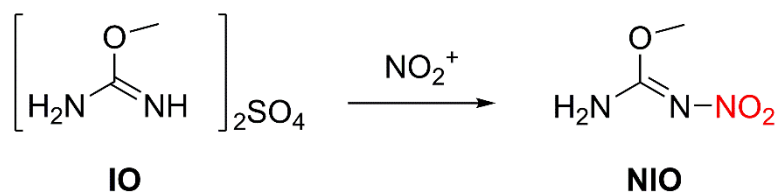
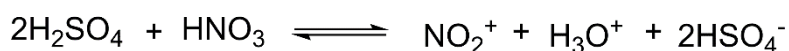
The determination of reaction orders was conducted using batch reactions for simplification. These reactions were executed in a water bath with magnetic stirring (MR Hei-Tec, Heidolph) and a 25 mL single-necked round-bottomed flask. Solution A was placed in the flask and heated to the designated reaction temperature. Solution B, also pre-heated to reaction temperature, was rapidly introduced into Solution A. The mixture was stirred at 1100 revolutions per minute to minimize the effect of external diffusion (Fig. S1).[28] Samples were periodically collected throughout the reaction process. Both batch and continuous flow reactions in this study were performed under isothermal conditions.

2.5 Kinetic modeling optimization process

The classical integral method was employed to determine the reaction order [29]. Various integral forms of kinetic equations corresponding to different reaction orders were fitted against the experimental data. The reaction orders yielding the highest R^2 were selected as the best fit. Subsequently, the least squares method was used to fit the kinetic data obtained under different reaction conditions, allowing for the determination of the pre-exponential factors and activation energies. Finally, the accuracy of the resulting kinetic model was validated through experimental testing.

3. Results and discussion

In this section, we perform kinetic modeling for the continuous-flow synthesis of NIO from IO and mixed acid (Scheme 1). The reaction was then optimized by kinetic modeling.



Scheme 1. Nitration of IO with mixed acid.

3.1 Prescreening experiments

The solubility of IO in H_2SO_4 is critical in ensuring the smooth progression of nitration reactions within a homogeneous system. Given the strongly exothermic nature of this reaction, an excessively high concentration of IO can lead to an overproduction of heat, thereby elevating the associated risks. In contrast, a concentration that is too low may fall beneath the detection threshold, compromising the reliability of the experimental data. To strike a balance, the initial concentration of IO was set to 0.5 mol/L in the reaction mixture. In addition, the effect of the molar ratio between the two reactants was examined. As shown in Fig. S2, the conversion of IO gradually increased as the molar ratio of HNO_3 elevated. The molar ratio of HNO_3 was established at 4.4 eq, a value chosen to optimize both conversion and atom efficiency.

3.2 Effect of two types of mixing equipment

Upon achieving homogeneous nitration conditions, our next objective was to eliminate the influence of mass transfer. We assessed the impact of flow rate on the reaction conversion under two distinct mixing scenarios (Figure 2a and 2c). The assessments were performed with reaction temperatures at 30-40 °C to eliminate the impact of the high viscosity of sulfuric acid [30]. Fig. 2a illustrates the scenario employing solely a T-mixer, and Fig. 2c shows the effect of flow rate on the conversion under this setup. Even when the flow rate was escalated to 14 mL/min, the conversion failed to stabilize

at a plateau, suggesting that mass transfer limitations had not been fully addressed. Conversely, with the addition of our homemade static mixer which consists of a 1/16-inch mixing coil and a SiO₂ beads-filled column (Fig. 2b), the conversion rate plateaued once the total flow rate surpassed 8 mL/min (Fig. 2d), suggesting the elimination of mass transfer limitations. The improved mixing efficiency can be attributed to the mixer's design features, such as its double reverse rotating vortex,[31, 32] large specific surface area,[33] and the incorporation of obstacles within the flow channel.[34, 35]

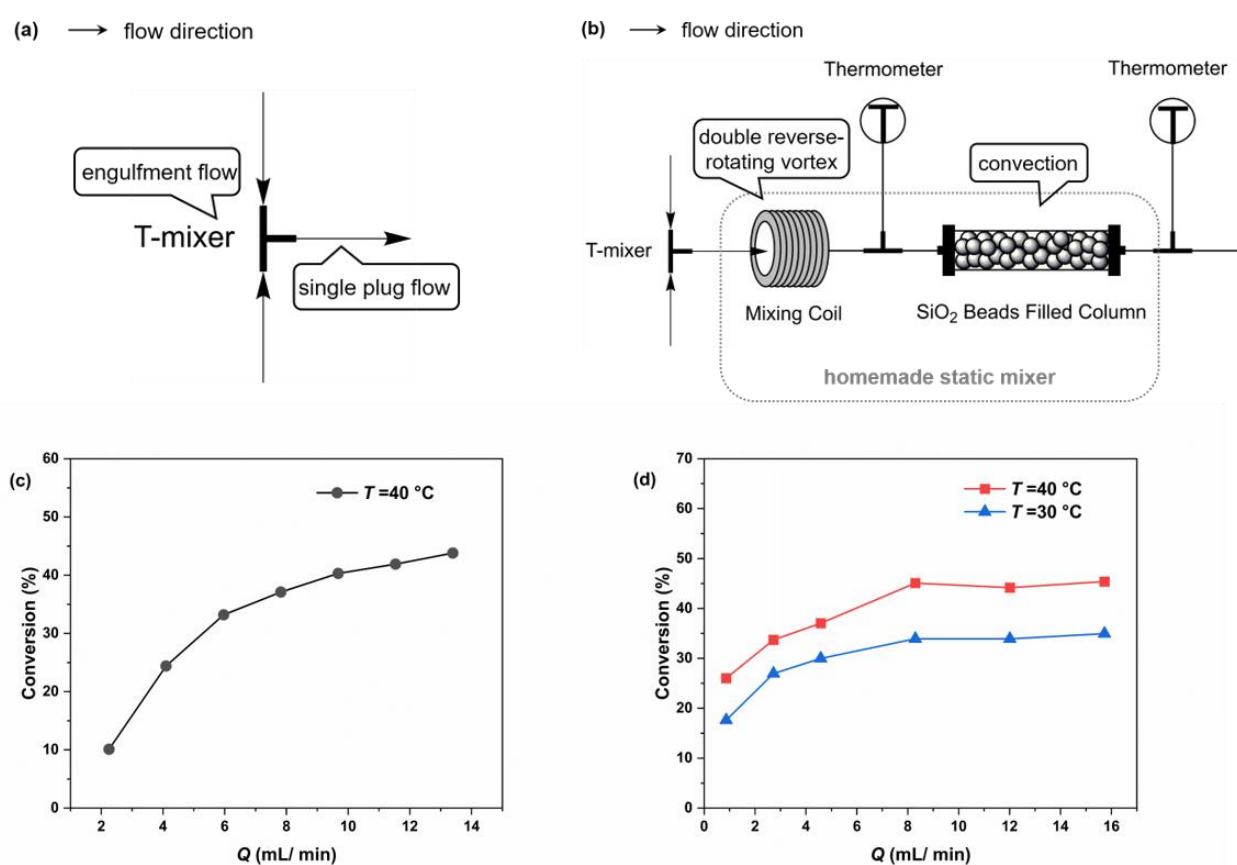


Figure 2. Two mixing setups: (a) a T-mixer and (b) a T-mixer combined with a homemade static mixer, and the effect of the two mixing setups on the mixing process; (c) the T-mixer and (d) the T-mixer plus the homemade static mixer effect of flow rate on conversion. Reaction conditions: H₂SO₄ mass fractions = 98 %, reaction temperature T = 40 °C, residence time $t = 2$ min, Initial concentration of reactants $C_{IO} = 1$ mol/L, $C_{HNO_3} = 4.4$ mol/L.

3.3 Determining reaction orders

In a batch reactor setup, the reaction orders of IO and HNO₃ were determined. The

initial concentration of HNO₃ was set at a level significantly higher (14 times greater) than that of IO. This approach allowed for the assumption that the concentration of HNO₃ remained constant throughout the reaction, enabling the conversion of the rate constant to K_β (Eq. 3). The relationship between reaction time and the conversion of IO was analyzed according to the first-order (Eq. 4) and second-order (Eq. 5) reaction kinetics, where x_{IO} represented the conversion of IO and t denoted the reaction time. The outcome of these fittings is presented in Fig. 3a for first-order and Fig. 3b for second-order. Notably, the higher R² observed in Fig. 3a compared to Fig. 3b suggests that the reaction of IO follows first-order kinetics.

$$-\frac{dC_{IO}}{dt} = kC_{IO}^\alpha C_{HNO_3}^\beta \approx K_\beta C_{IO}^\alpha \quad (3)$$

$$\ln(1 - x_{IO}) = -K_\beta t \quad (4)$$

$$\frac{1}{1-x_{IO}} = 1 + K_\beta t \quad (5)$$

Given that the reaction order of IO was determined to be 1, Eq. 3 was subsequently transformed into Eq. 6. As nitration reactions are predominantly second-order, we explored the potential for the reaction order of HNO₃ (β) to be either 0 or 1 by fitting the reaction data to Eq. 7 and Eq. 8, respectively.

$$-\frac{dC_{IO}}{dt} = kC_{IO}C_{HNO_3}^\beta \quad (6)$$

$$\ln(1 - x_{IO}) = -K_\beta t \quad (7)$$

$$\frac{1}{C_{HNO_3 0} - C_{IO 0}} \ln\left(\frac{1 - x_{HNO_3}}{1 - x_{IO}}\right) = -K t \quad (8)$$

The fitting results, as depicted in Fig. 3c for $\beta=0$ and Figure 3d for $\beta=1$, revealed that R² for the latter scenario (R²=0.988) was higher than that for the former (R²=0.974). This outcome indicates that the reaction order of HNO₃ is also 1, which transforms Eq. 6 to Eq. 9.

$$-\frac{dC_{IO}}{dt} = kC_{IO}C_{HNO_3} \quad (9)$$

Also, with $M = \frac{C_{\text{HNO}_3^0}}{C_{\text{IO}_0}}$, Eq. 8 can be rewritten to Eq. 10.

$$\ln \left[\frac{M - x_{\text{IO}}}{M(1 - x_{\text{IO}})} \right] = (M - 1)C_{\text{IO}_0}kt \quad (10)$$

After the reaction order being determined, all the rest of experiments were conducted in the continuous flow reactor, and the t in Eq. 10 refers to residence time.

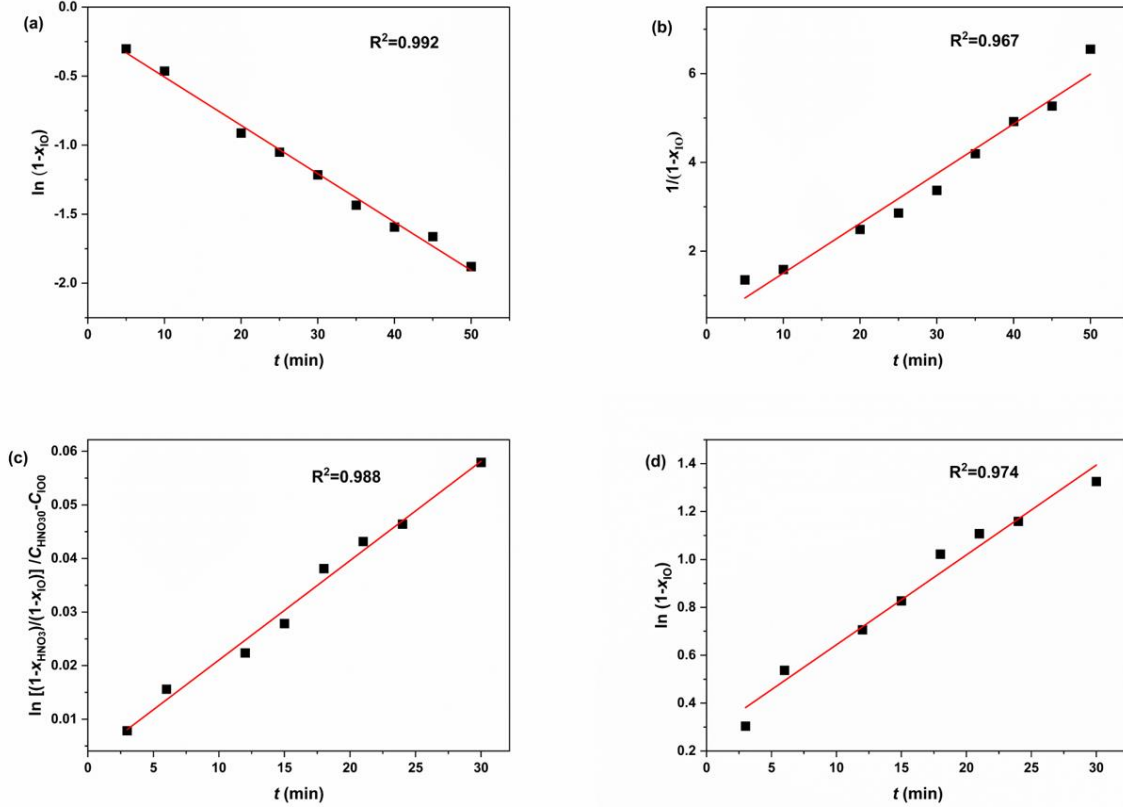


Figure 3. Determination of the number of reaction orders. (a). $\ln(1 - x_{\text{IO}})$ versus t ; (b). $\frac{1}{1 - x_{\text{IO}}}$ versus

t ; (c). $\ln(1 - x_{\text{IO}})$ versus t ; (d). $\frac{1}{C_{\text{HNO}_3^0} - C_{\text{IO}^0}} \ln \left(\frac{1 - x_{\text{HNO}_3}}{1 - x_{\text{IO}}} \right)$ versus t . Reaction condition for

determining IO's reaction order: H_2SO_4 mass fractions = 98 %, reaction temperature (T) = 0 °C; initial concentration of reactants in reaction mixture: $C_{\text{IO}_0} = 1$ mol/L, $C_{\text{HNO}_3^0} = 15$ mol/L; stirring speed = 1100 rpm. Reaction condition for determining HNO_3 's reaction order: reaction temperature (T) = 0 °C; initial concentration of reactants in reaction mixture: $C_{\text{NIO}_0} = 1$ mol/L, $C_{\text{HNO}_3^0} = 4.4$ mol/L; stirring speed = 1100 rpm.

3.4 Determining the apparent reaction kinetics

The variation in the conversion of IO (x_{10}) as the function of time (t) at different temperatures (30 °C, 35 °C, 40 °C) and H₂SO₄ mass fractions (88 %, 90 %, 92 %, 94%, 96 %, and 98 %) is depicted in Fig. S3 and subsequently modeled using Eq. 10. The fitting results shown in Fig. 4 exhibit robust linear correlations ($R^2 > 0.99$), facilitating the calculation of rate constants based on the slopes of these lines across the varied temperatures and H₂SO₄ concentrations. Table 1 indicates that the reaction rate constants escalate with increasing H₂SO₄ mass fraction, which aligns with findings from previous studies on mixed-acid catalyzed nitration reactions [36, 37]. However, the data also reveal a decline in rate constants when the H₂SO₄ mass fraction exceeds 94 %, suggesting a complex interaction at higher acid concentrations.

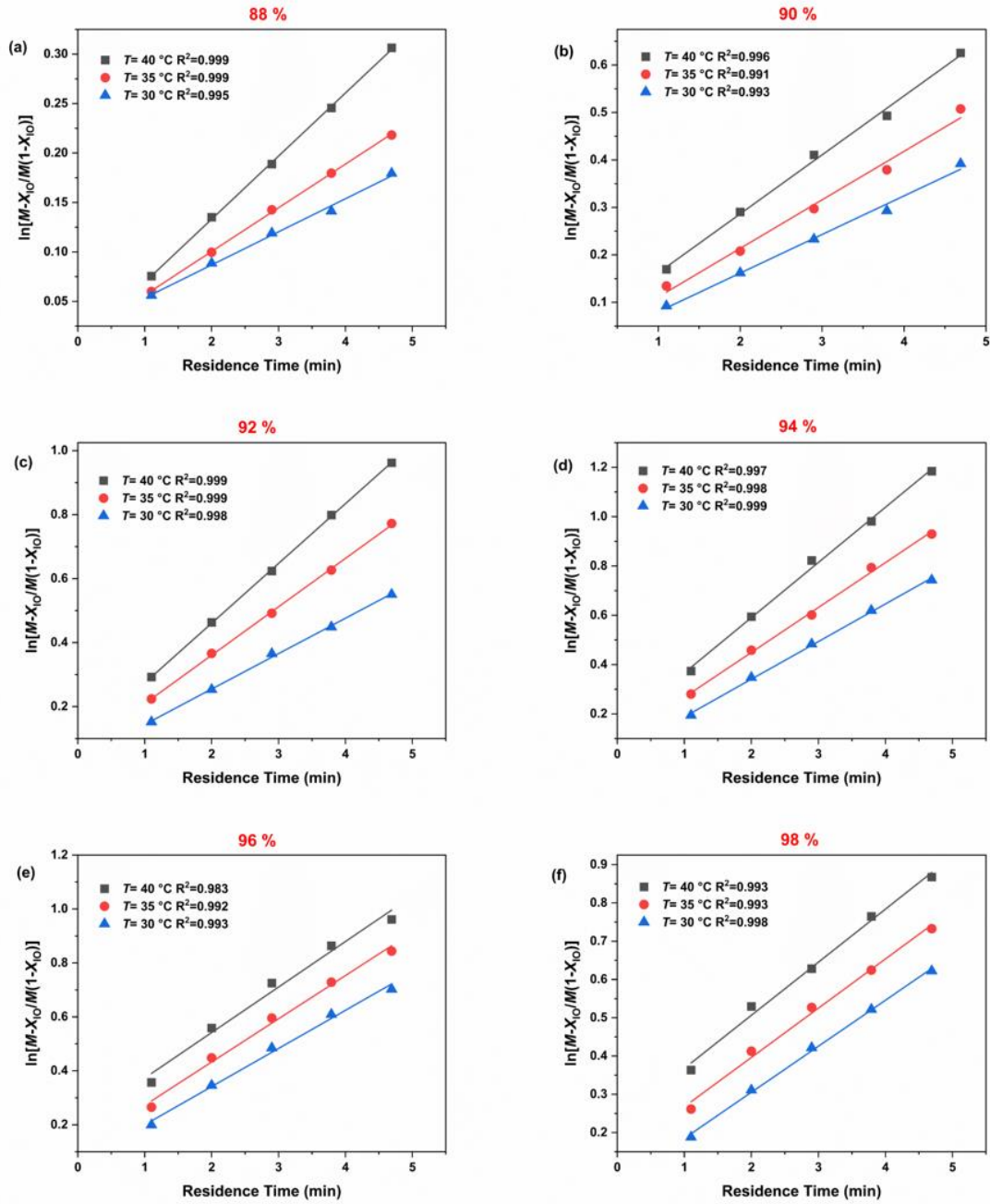


Figure 4. Determination of $(M - 1)C_{100}k$ at different temperatures and H₂SO₄ mass fractions. (a) 88 % H₂SO₄, (b) 90 % H₂SO₄, (c) 92 % H₂SO₄, (d) 94 % H₂SO₄, (e) 96 % H₂SO₄, and (f) 98 % H₂SO₄.

Table 1. Values of k for different H₂SO₄ mass fractions and at different temperature

Mass fraction of H ₂ SO ₄ (wt %)	$k \times 10^2$ (L/mol/s)		
	30 °C	35 °C	40 °C
88	2.26	2.98	4.31
90	5.51	6.91	8.40
92	7.48	10.2	12.6
94	10.3	12.3	15.1
96	9.56	10.8	11.4
98	8.13	8.70	9.37

3.5 Determining the intrinsic reaction kinetics

Given the strong correlation between the observed HNO₃-based reaction rate constant and the H₂SO₄ mass fraction, intrinsic reaction constants independent of H₂SO₄ concentration were determined to study the intrinsic kinetics of the reaction. Previous research has established that the relationship between the apparent and intrinsic kinetics of nitrification can be described by Eq. 11.[17, 38]

$$\lg k = \lg \left(\frac{C_{\text{NO}_2^+}}{C_{\text{HNO}_3}} \right) + nM_C + \lg k_0 \quad (11)$$

where k_0 is the intrinsic rate constant only based on NO₂⁺ and independent of sulfuric acid concentration,[39] n is a thermodynamic parameter related to the type of compound, and M_C is the activity coefficient function introduced in the next section.

By shifting the terms in Eq. 11, Eq. 12 can be obtained as:

$$\lg k - \lg \left(\frac{C_{\text{NO}_2^+}}{C_{\text{HNO}_3}} \right) = nM_C + \lg k_0 \quad (12)$$

Therefore, by plotting $\lg k - \lg \left(\frac{C_{\text{NO}_2^+}}{C_{\text{HNO}_3}} \right)$ as the vertical coordinate and M_C as the horizontal coordinate, the values of n and k_0 can be obtained from the slope and intercept of the resulting fitting line. Since the values of M_C and $\lg \left(\frac{C_{\text{NO}_2^+}}{C_{\text{HNO}_3}} \right)$ change

with the change in sulfuric acid temperature and mass fraction, we determine the values of M_C and $\lg\left(\frac{C_{\text{NO}_2^+}}{C_{\text{HNO}_3}}\right)$ according to the method proposed by Luo et al.[17, 38]. As the ranges of sulfuric acid concentrations and temperature in our study were different from Luo et al.'s study, recalculations were required to obtain the values of M_C and $\lg\left(\frac{C_{\text{NO}_2^+}}{C_{\text{HNO}_3}}\right)$.

3.5.1 Determination of M_C values

The value of M_C can be calculated using Eq. 13 and 14. Eq. 13 [40] was employed to predict M_C at various H_2SO_4 concentrations at 298K, specifically when the H_2SO_4 concentration is between 15.2 and 18.4 mol/L. By fitting the predicted data, M_C as a function of H_2SO_4 concentration at a given temperature was determined (Fig. S5). In addition, the values of M_C for different sulfuric acid concentrations at a given temperature can be obtained by substituting the corresponding temperature into Eq.14, as first introduced by Marziano et al.

$$-M_C(298\text{K}) = 2.16 \times 10^{-4}C_{\text{H}_2\text{SO}_4}^5 - 1.27 \times 10^{-2}C_{\text{H}_2\text{SO}_4}^4 + 0.28C_{\text{H}_2\text{SO}_4}^3 - 2.73C_{\text{H}_2\text{SO}_4}^2 + 10.6C_{\text{H}_2\text{SO}_4} \quad (13)$$

$$M_C(T) = M_C(298\text{K}) \left[\frac{200}{T} + 0.3292 \right] \quad (14)$$

3.5.2 Determination of $\lg\left(\frac{C_{\text{NO}_2^+}}{C_{\text{HNO}_3}}\right)$ values

Since NO_2^+ is the actual reactive species in the nitration reaction [14], an accurate estimation of its concentration is essential for the study of intrinsic kinetics. Based on the values of $\frac{C_{\text{NO}_2^+}}{C_{\text{HNO}_3}}$, reported in previous studies for different temperatures and sulfuric acid concentrations [41-43], the mass fraction of sulfuric acid was plotted against $\lg\left(\frac{C_{\text{NO}_2^+}}{C_{\text{HNO}_3}}\right)$. The fitting results shown in Fig. 5a exhibit robust linear correlations, enabling the calculation of $\lg\left(\frac{C_{\text{NO}_2^+}}{C_{\text{HNO}_3}}\right)$ at temperatures of 23 °C, 40 °C, and 60 °C. Subsequently, by plotting $\lg\left(\frac{C_{\text{NO}_2^+}}{C_{\text{HNO}_3}}\right)$ versus $1/T$, a series of fitted curves for the

studied range of sulfuric acid concentrations (88-98 wt%) can be obtained, as shown in Fig. 5b. Thus, the values of $\lg\left(\frac{C_{\text{NO}_2^+}}{C_{\text{HNO}_3}}\right)$ at different sulfuric acid concentrations and temperatures can be determined.

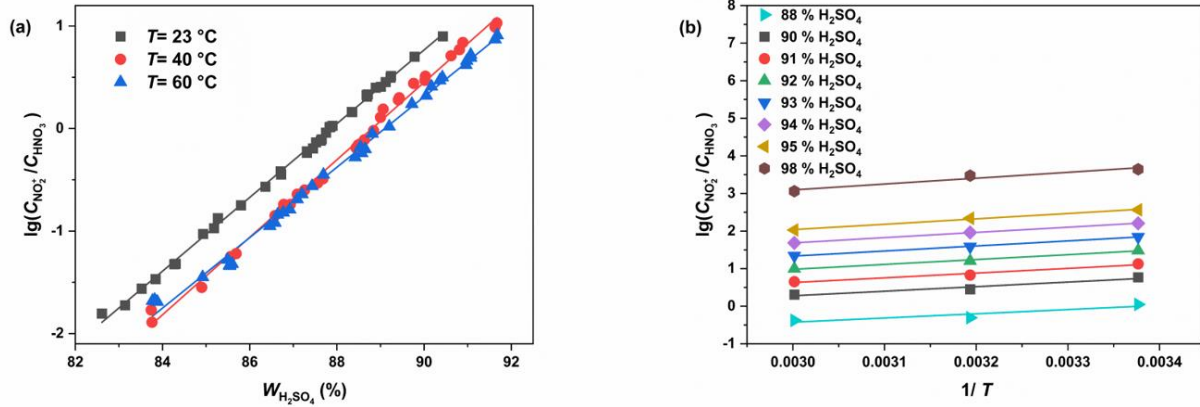


Figure 5. Variations and fitting of as a function of (a). the mass fraction of H₂SO₄ at 23 °C, 40 °C, and 60 °C; (b). 1/ T at different H₂SO₄ concentrations $\lg\left(\frac{C_{\text{NO}_2^+}}{C_{\text{HNO}_3}}\right)$.

3.5.3 Determination of intrinsic kinetic parameters

With $\lg\left(\frac{C_{\text{NO}_2^+}}{C_{\text{HNO}_3}}\right)$ and M_C at different conditions determined in Fig. 5, $\lg k - \lg\left(\frac{C_{\text{NO}_2^+}}{C_{\text{HNO}_3}}\right)$ was plotted against M_C at different temperatures (Fig. 6a-c), and fitting these data into Eq. 12 lead to ($R^2 > 0.99$). The values of k_0 and n at different temperatures are shown in Table 2. The value of k_0 increases with increasing temperature and the value of n remains almost constant with temperature, which is consistent with the results reported in previous studies for other mixed acid-catalyzed nitration reactions.[15, 44]

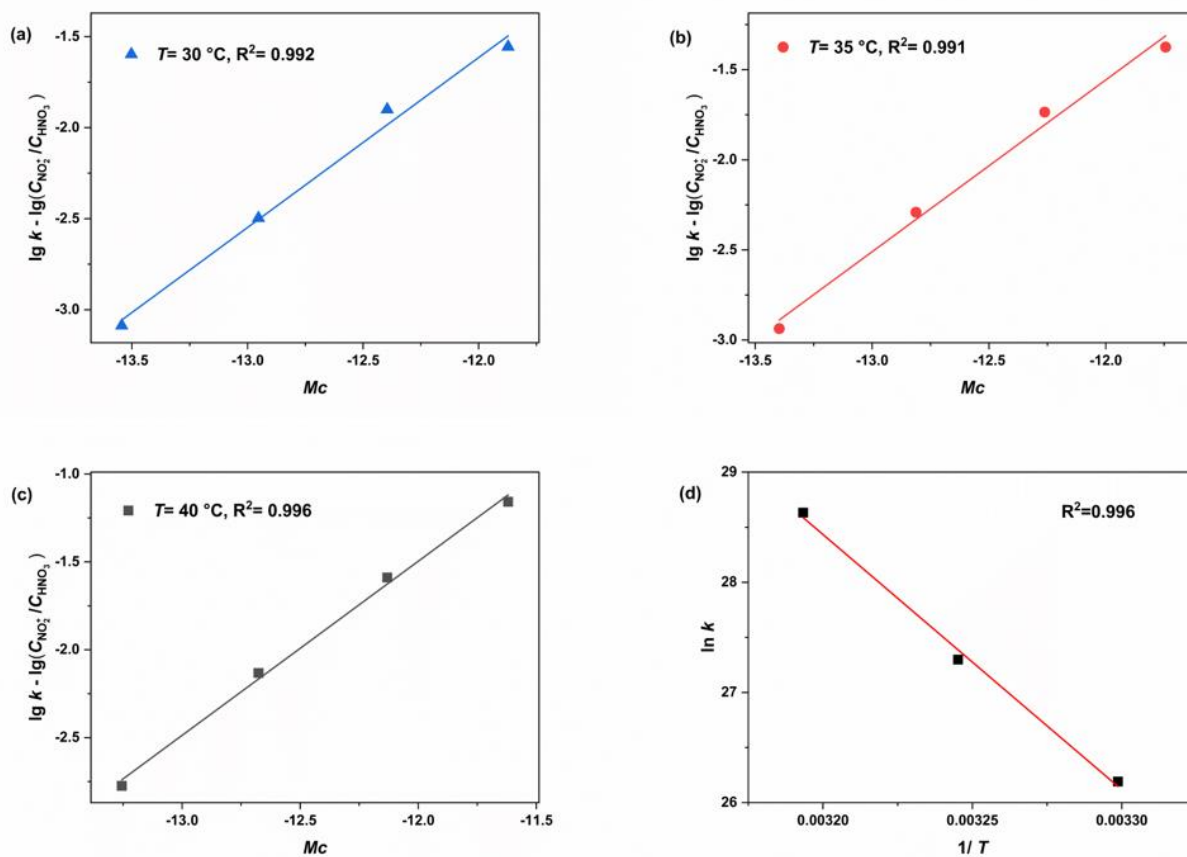


Figure 6. Determination of thermodynamic parameters n and k_0 and determination of activation energy and pre-exponential factors.

Table 2. Values of n and $\lg k_0$ at different temperatures

Temperature ($^\circ\text{C}$)	n	$\lg k_0$
30	1.0764	11.3749
35	1.1127	11.8556
40	1.1577	12.4352

According to the values of k_0 at different temperatures, the activation energy for the electrophilic attack of NO_2^+ on the IO can be calculated by the Arrhenius equation:

$$\ln k_0 = -\frac{E_a}{RT} + \ln A \quad (17)$$

where R is the molar gas constant and T denotes the temperature in Kelvin, and E_a and A are the activation energy and pre-exponential factors for the IO nitration.

By fitting $\ln k_0$ versus $1/T$ into Eq. 17 (Fig. 6d), the value of E_a and $\ln A$ was determined (Table 3).

Table 3. Values of the pre-exponential factors and activation energy

Factors	E_a (kJ/mol)	$\ln A$
Values	192.57	102.55

3.6 The synergic effect of temperature and sulfuric acid concentration on the apparent kinetics

As discussed above, the apparent rate constant is determined by three components, $\lg\left(\frac{C_{\text{NO}_2^+}}{C_{\text{HNO}_3}}\right)$, nM_C , and $\lg k_0$. First, the intrinsic rate constant k_0 that is only temperature-dependent and is not affected by the concentration of sulfuric acid (Eq. 11). In addition, Fig. 5b shows that $\lg\left(\frac{C_{\text{NO}_2^+}}{C_{\text{HNO}_3}}\right)$ increases with the increase in sulfuric acid concentration when the temperature is fixed. In contrast, nM_C is a negative value that decreases with higher sulfuric acid concentration (Table S1). As the concentration of sulfuric acid increases, the decrease in nM_C gradually surpassed the increase in $\lg\left(\frac{C_{\text{NO}_2^+}}{C_{\text{HNO}_3}}\right)$ when the sulfuric acid concentration exceeded 94%, resulting in an overall decrease of k (Fig. 7a). Similar trends were reported in the nitration of nitrobenzene[45] and *o*-nitrotoluene[16], suggesting that the phenomenon observed in our study is not isolated.

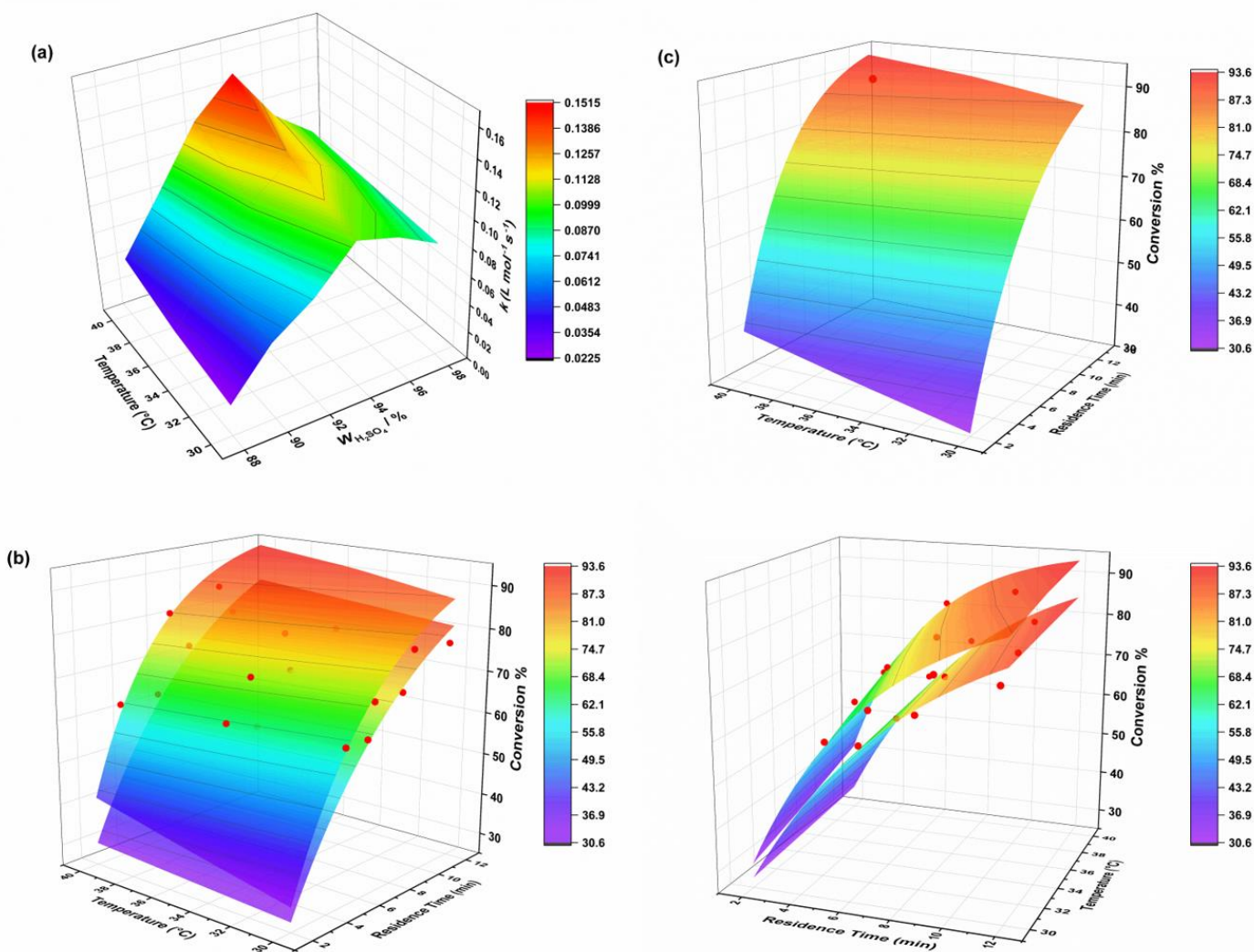


Figure 7. (a). The value of apparent rate constant k at various H_2SO_4 mass fractions and different temperatures. (b). Validation of reaction kinetic models with different mass fractions of sulfuric acid. (From top to bottom, the theoretical response surfaces and experimental values are shown for sulfuric acid mass fractions of 94 % and 98 %, respectively.) (c). Response surface of the kinetic model under optimized conditions and experimental results.

3.7 Validation of kinetic models

Based on the IO intrinsic nitration kinetic model, we plotted the response surfaces of the predicted conversion of IO at different temperatures and different residence times under different mass fractions of sulfuric acid (94 % H_2SO_4 and 98 % H_2SO_4) by designing a series of validation experiments. The result is shown in Fig. 7b, with a temperature range of 30-40 °C and a time range of 4-12 min. For example, a conversion

predicted to be 80 % under conditions of 94 % H₂SO₄ and 6.33 minutes at 40 °C was actually 81.1 %, and a conversion forecasted at 70 % for 98 % H₂SO₄ and 8.58 minutes at 25 °C ended up being 69.3 %. The predicted conversion rates are in good agreement with the experimental ones (red dots).

3.8 Reaction optimization using kinetic models

From the study of the intrinsic kinetics of IO nitric acid, it is known that the reaction rate is affected by the intrinsic rate constant, sulfuric acid activity coefficient function, and the concentration of NO₂⁺. The apparent rate constant increases and then decreases with increasing sulfuric acid mass fraction in the range of 88-98 %. We chose the sulfuric acid concentration (94 wt %), which has the largest apparent rate constant, as the optimized reaction condition to accelerate the rate of IO nitric acid. In addition, higher temperatures and longer residence times also contribute to the conversion rate. We chose the highest temperature within the kinetic model cover (30-40 °C) as the optimization condition and extended the validated reaction time range (4-12 min) to a certain extent. Therefore, the optimized reaction conditions for NIO were obtained by the response surface of kinetic modeling (Fig. 7c): the sulfuric acid mass fraction was 94 %, the initial concentration of IO was 0.5 mol/L, the reaction temperature was 40 °C, the molar ratio was 4.4:1, and the reaction time was 12.36 min. Under this condition, the experimentally measured conversion was 87.4 %, shown as the red dot in Fig. 7c.

4. Conclusion

In this work, a homogeneous nitration system for the synthesis of *O*-methyl-*N*-nitroisourea was constructed. To eliminate the mass transfer resistance between the two liquid phases during the reaction, a homemade simple and effective static mixer was used which rapidly achieved thorough mixing of the two phases with little temperature fluctuation. The effects of temperature, residence time, and sulfuric acid mass fraction on the reaction were investigated as well as the apparent and intrinsic rate constants based on nitric acid and NO₂⁺ observations were obtained, respectively. The apparent

rate constants observed based on nitric acid are highly correlated with the mass fraction of sulfuric acid, increasing and then decreasing as the mass fraction of sulfuric acid increases, with 94 % sulfuric acid being the turning point. This is the result of a combination of the intrinsic rate constant, the sulfuric acid activity coefficient function, and the NO_2^+ concentration. Thus, the effect of different sulfuric acid mass fractions and temperatures on the apparent rate constants can be understood. In addition, a complete kinetic model of IO nitration based on NO_2^+ was developed to describe the reaction process, the activation energy of the IO nitration was calculated to be 192.57 kJ/mol. Furthermore, the accuracy of the kinetic model was verified by comparing the predicted data with the experimental data. Finally, the reaction was optimized by kinetic modeling and 87.4 % conversion of IO was achieved under optimum conditions. This kinetic model can be used to understand the nitration process of IO and optimize the reactor design, which can serve as guidance for industrial production.

Declaration of Competing Interest

The authors declare that they have no known competing financial interests or personal relationships that could have appeared to influence the work reported in this paper.

Acknowledgments

This research was supported by the Joint Funds of the Zhejiang Provincial Natural Science Foundation of China under Grant No. LHDMZ23B060001, Zhejiang Province Science and Technology Plan Project under Grant No. 2022C01179, and the National Natural Science Foundation of China under Grant No. 22108252.

References

1. Elbert, A.; Haas, M.; Springer, B.; Thielert, W.; Nauen, R. *Pest Manage. Sci.* **2008**, *64* (11), 1099–1105, 10.1002/ps.1616.
2. Uneme, H.; Konobe, M.; Ishizuka, H.; Kamiya, Y. Preparation of heteroarylmethylisoureas and related compounds. Pat. Appl. Copyright (C) 2023

- American Chemical Society (ACS). All Rights Reserved., Pat. WO9700867A1, 1997.
3. Uneme, H.; Kamiya, Y.; Konobe, M.; Yamada, J. Manufacture of *N*-(heterocyclylmethyl)-*N'*-nitroisoureas. Pat. Appl. Copyright (C) 2023 American Chemical Society (ACS). All Rights Reserved., Pat. WO9933809A1, 1999.
 4. Brady, J. F.; Simmons, D. P.; Wilson, T. E. Immunoassay for neonicotinoid insecticides. Pat. Appl. Copyright (C) 2023 American Chemical Society (ACS). All Rights Reserved., Pat. WO2001042787A2, 2001.
 5. Köckinger, M.; Wyler, B.; Aellig, C.; Roberge, D. M.; Hone, C. A.; Kappe, C. O. *Org. Process Res. Dev.* **2020**, *24* (10), 2217–2227, 10.1021/acs.oprd.0c00254.
 6. Magosso, M.; van den Berg, M.; van der Schaaf, J. *React. Chem. Eng.* **2021**, *6* (9), 1574–1590, 10.1039/D1RE00141H.
 7. Sheng, L.; Chen, Y.; Wang, K.; Deng, J.; Luo, G. *Chem. Eng. Sci.* **2021**, *239*, 116621, 10.1016/j.ces.2021.116621.
 8. Sheng, L.; Ma, L.; Chen, Y.; Deng, J.; Luo, G. *Chem. Eng. J.* **2022**, *427*, 132067, 10.1016/j.cej.2021.132067.
 9. Guo, S.; Zhan, L.-w.; Li, B.-d. *Chem. Eng. J.* **2023**, *468*, 143468, 10.1016/j.cej.2023.143468.
 10. Jin, N.; Song, Y.; Yue, J.; Wang, Q.; Lu, P.; Li, Y.; Zhao, Y. *Chem. Eng. Sci.* **2023**, *281*, 119198, 10.1016/j.ces.2023.119198.
 11. Rahaman, M.; Mandal, B. P.; Ghosh, P. *Am. Inst. Chem. Eng.* **2007**, *53* (9), 2476–2480, 10.1002/aic.11222.
 12. Taylor, C. J.; Pomberger, A.; Felton, K. C.; Grainger, R.; Barecka, M.; Chamberlain, T. W.; Bourne, R. A.; Johnson, C. N.; Lapkin, A. A. *Chem. Rev.* **2023**, *123* (6), 3089–3126, 10.1021/acs.chemrev.2c00798.
 13. Yao, Z.; Xu, X.; Dong, Y.; Liu, X.; Yuan, B.; Wang, K.; Cao, K.; Luo, G. *Chem. Eng. Sci.* **2020**, *228*, 115892, 10.1016/j.ces.2020.115892.
 14. Hughes, E. D.; Ingold, C. K.; Reed, R. I. *Nature* **1946**, *158* (4013), 448–449, 10.1038/158448c0.
 15. Cui, Y.; Song, J.; Du, C.; Deng, J.; Luo, G. *Am. Inst. Chem. Eng.* **2022**, *68* (4), e17564, 10.1002/aic.17564.
 16. Song, J.; Cui, Y.; Luo, G.; Deng, J.; Wang, Y. *React. Chem. Eng.* **2022**, *7* (1), 111–122, 10.1039/D1RE00362C.
 17. Song, J.; Cui, Y.; Sheng, L.; Wang, Y.; Du, C.; Deng, J.; Luo, G. *Chem. Eng. Sci.* **2022**, *247*, 117041, 10.1016/j.ces.2021.117041.
 18. Dessimoz, A.-L.; Cavin, L.; Renken, A.; Kiwi-Minsker, L. *Chem. Eng. Sci.* **2008**, *63* (16), 4035–4044, 10.1016/j.ces.2008.05.005.
 19. Hessel, V.; Löwe, H.; Schönfeld, F. *Chem. Eng. Sci.* **2005**, *60* (8), 2479–2501, 10.1016/j.ces.2004.11.033.
 20. Zhang, S.; Zhu, C.; Feng, H.; Fu, T.; Ma, Y. *Chem. Eng. Sci.* **2021**, *229*, 116040, 10.1016/j.ces.2020.116040.
 21. Holvey, C. P.; Roberge, D. M.; Gottsponer, M.; Kockmann, N.; Macchi, A. *Chem. Eng. Process.* **2011**, *50* (10), 1069–1075, 10.1016/j.cep.2011.05.016.
 22. Tajik Ghanbari, T.; Rahimi, M.; Ranjbar, A. A.; Pahamli, Y.; Torbatinejad, A. *Phys. Fluids* **2023**, *35* (12), 10.1063/5.0177344.

23. Al-Azzawi, M.; Mjalli, F. S.; Husain, A.; Al-Dahhan, M. *Ind. Eng. Chem. Res.* **2021**, *60* (14), 5049–5075, 10.1021/acs.iecr.0c05858.
24. Bhagat, A. A. S.; Peterson, E. T. K.; Papautsky, I. *J. Micromech. Microeng.* **2007**, *17* (5), 1017, 10.1088/0960-1317/17/5/023.
25. Su, Y.; Chen, G.; Yuan, Q. *Chem. Eng. Sci.* **2011**, *66* (13), 2912–2919, 10.1016/j.ces.2011.03.024.
26. Santana, H. S.; Silva, J. L., Jr.; da Silva, A. G. P.; Rodrigues, A. C.; Amaral, R. d. L.; Noriler, D.; Taranto, O. P. *Ind. Eng. Chem. Res.* **2021**, *60* (25), 9216–9230, 10.1021/acs.iecr.1c00770.
27. Kilcher, E.; Freymond, S.; Vanoli, E.; Marti, R.; Schmidt, G.; Abele, S. *Org. Process Res. Dev.* **2016**, *20* (2), 432–439, 10.1021/acs.oprd.5b00046.
28. Russo, D.; Tomaiuolo, G.; Andreatti, R.; Guido, S.; Lapkin, A. A.; Di Somma, I. *Chem. Eng. J.* **2019**, *377*, 120346, 10.1016/j.cej.2018.11.044.
29. Xu, Q.; Fan, H.; Yao, H.; Wang, D.; Yu, H.; Chen, B.; Yu, Z.; Su, W. *Chem. Eng. J.* **2020**, *398*, 125584.
30. Dunstan, A. E. *Proc. Chem. Soc., London* **1914**, *30*, 104–5.
31. Dean, W. R.; Hurst, J. M. *Mathematika* **1959**, *6* (1), 77–85, 10.1112/S0025579300001947.
32. Jonas Bolinder, C.; Sundén, B. *Exp. Therm. Fluid Sci.* **1995**, *11* (4), 348–363, 10.1016/0894-1777(95)00040-2.
33. Lü, Y.; Zhu, S.; Wang, K.; Luo, G. *Chin. J. Chem. Eng.* **2016**, *24* (6), 711–718, 10.1016/j.cjche.2016.01.011.
34. Tata Rao, L.; Goel, S.; Kumar Dubey, S.; Javed, A. *J. Phys.: Conf. Ser.* **2019**, *1276* (1), 012003, 10.1088/1742-6596/1276/1/012003.
35. Bazargan-Lari, Y.; Movahed, S.; Mashhoodi, M. *J. Mech.* **2016**, *33* (3), 387–394, 10.1017/jmech.2016.81.
36. Li, S.; Zhang, X.; Ji, D.; Wang, Q.; Jin, N.; Zhao, Y. *Chem. Eng. Sci.* **2022**, *255*, 117657, 10.1016/j.ces.2022.117657.
37. Yang, M.; Liao, C.; Tang, C.; Zhang, P.; Huang, Z.; Li, J. *Phys. Chem. Chem. Phys.* **2021**, *23* (8), 4658–4668, 10.1039/DOCP05935H.
38. Cui, Y.; Song, J.; Du, C.; Deng, J.; Luo, G. *AIChE J.* **2022**, *68* (4), e17564, 10.1002/aic.17564.
39. Olah, G. A.; Malhotra, R.; Narang, S. C. NITRATION: Methods and Mechanisms. In *Across Conventional Lines*; 1989; pp 975–979.
40. Marziano, N. C.; Tomasin, A.; Traverso, P. G. *J. Chem. Soc., Perkin Trans. 2* **1981**, (7), 1070–1075, 10.1039/P29810001070.
41. Deno, N. C.; Peterson, H. J.; Sacher, E. *J. Phys. Chem.* **1961**, *65* (2), 199–201, 10.1021/j100820a002.
42. C. Marziano, N.; Tomasin, A.; Tortato, C.; M. Zaldivar, J. *J. Chem. Soc., Perkin Trans. 2* **1998**, (9), 1973–1982, 10.1039/A802521E.
43. Ross, D. S.; Kuhlmann, K. F.; Malhotra, R. *J. Am. Chem. Soc.* **1983**, *105* (13), 4299–4302, 10.1021/ja00351a030.
44. Wen, Z.; Yang, M.; Zhao, S.; Zhou, F.; Chen, G. *React. Chem. Eng.* **2018**, *3* (3), 379–387, 10.1039/C7RE00182G.

45. Rahaman, M. ; Mandal, B. ; Ghosh, P. *Am. Inst. Chem. Eng.* **2010**, *56* (3), 737-748, 10.1002/aic.11989.